The 38th Annual Asilomar Conference on Signals, Systems, and Computers
Pacific Grove CA, USA, Nov. 7–10, 2004, http://web.nps.navy.mil/ asilomar

Three-Phase Sample Timing on a Wideband Triangular Array of 4/3 the Usual Density Reduces the Nyquist Rate for Far-Field Signals by Two Thirds

Jeffrey O. Coleman
http://alum.mit.edu/www/jeffc

Naval Research Laboratory (http://www.nrl.navy.mil/)
Radar Division, Signal Processing Theory & Methods Section

Abstract

RF-sampled microwave arrays are often limited by the analog-digital conversion speed available. Here the nominally required speed is reduced by a factor of three without aliasing of far-field plane-wave information by using three sample-timing phases on a triangular planar array with 4/3 the element density of the usual "optimal" element layout.

1: Introduction

Ajdler and Vetterli [1] recently observed that for a microphone line array, position-dependent sampling can halve the sampling rate required to support a given signal bandwidth: (sampling instant, microphone position) coordinate pairs are taken from a carefully chosen quincunx lattice. This author independently rediscovered the principle a year later in the context of antenna arrays [2] and observed that the concept applies to both transmit and receive arrays, is compatible with both lowpass and bandpass sampling, and can involve analog up- or down-conversion between data conversion and the array. The usual element-spacing bound of half a wavelength at the upper RF band edge is replaced with a quarter-wavelength bound at the center of the Nyquist sampling band referred to RF, a reduction only for bandpass sampling. A subsequent paper [3] presented the associated upsampling beamformer structure for the receive version of the array and stepped through the process of designing the pattern. Transmit-array pattern design involves decimation and parallels the receive case.

This paper extends these ideas to a planar array, where the extra dimension offers many design options. Here an RF-sampled receive array is examined, but adapting these ideas to a transmit array or to an array with digital-analog conversion at IF should be straightforward using the linear-array development [2] as a model. The pattern-design process of [3] should likewise extend straightforwardly.

This work was supported by the Naval Research Laboratory funding base.

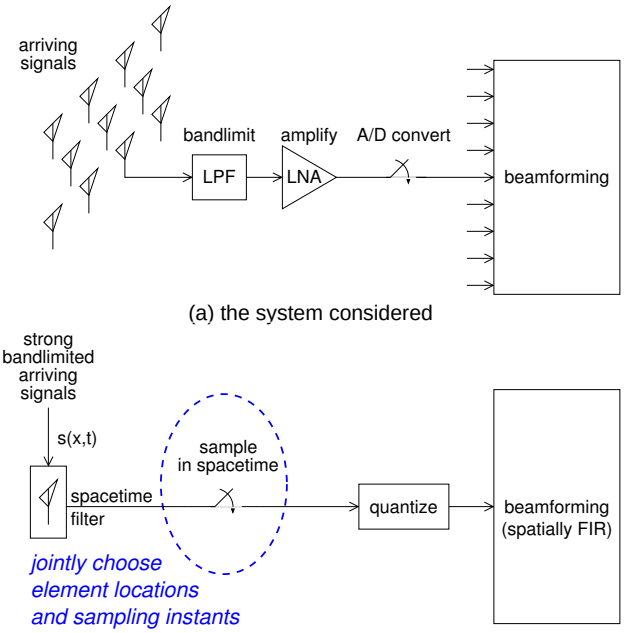

Figure 1: The receive system examined uses identical pre-beamforming processing on each element of a planar array of antenna elements. Element location and sample timing can be viewed together as an equivalent spactime-sampling operation, the Nyquist limits for which are examined in this paper.

The system of present interest, sketched in Fig. 1(a), will be viewed in the analysis below as the mathematically equivalent system of Fig. 1(b), where the element pattern is viewed as a linear, shift-invariant filter in two spatial dimensions and time. This step is analogous to factoring the element pattern out of the array pattern in the derivation of the array factor. Spacetime sampling as shown produces an array of 3D samples infinite in time and space, but the beamformer response is spatially finite (FIR) and so requires only a finite number of actual array elements.

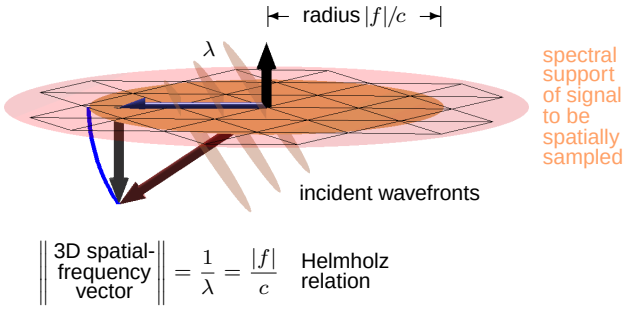

Figure 2: Geometry of the 2D spatial frequency (blue, horizontal).

2: A Little Review

Before addressing spacetime sampling, let's review spatial sampling to establish some conventions and to illustrate in 2D the design process that will later serve us well in 3D. Both developments rely fully on the far-field signal structure required by Maxwell's equations: a spectral continuum of plane-wave components propagating at velocity c.

In Fig. 2 an electromagnetic plane wave is incident at frequency f on a horizontal array plane. The wave's 3D spatial-frequency vector has length $|f|/c$ and points in the direction of propagation, from upper right to lower left. Spacetime filtering by the element pattern has presumably affected the wave's complex amplitude, but it cannot change this spatial-frequency vector. Now when this spacetime-filtered incident wave is sampled by the array plane, the resulting 2D wave has a spatial frequency that is just the projection into the plane of the original 3D spatial-frequency vector. This 2D vector must lie in the copper-colored circle. Further, if $|f|$ is known and if physical blockage of signals from below implies that the wave is from above, the one-to-one correspondence between the 2D vector's precise position in the circle and the wave's 3D direction of arrival makes these two quantities effectively equivalent.

The "$\leftrightarrow$" notation in Fig. 3 denotes a Fourier pair in a special sense. Positions in the array plane are represented on the left, and 2D spatial frequencies of waves in that plane are represented on the right. The circle containing these spatial frequencies, derived in Fig. 2, is shown on the right in Fig. 3(a), corresponding to all possible incident waves when they are sampled only by the plane itself, *i.e.* when the fields are (field component of interest is) known everywhere in the plane. In Fig. 3(b) those fields are presumed further sampled on the lattice of sample positions denoted by dots. Mathematically, those positions can be obtained as the product, shown below the axes on the left, of a sample-interval matrix with all possible values of a two-element integer vector $\left[\begin{smallmatrix} n_1 \\ n_2 \end{smallmatrix}\right]$. This spatial sampling of the signal causes its spatial spectrum to be infinitely replicated, with replica translates given by the product shown on the right of a spectral-period matrix with an arbitrary two-element integer vector $\left[\begin{smallmatrix} k_1 \\ k_2 \end{smallmatrix}\right]$. Depending on the coordinate

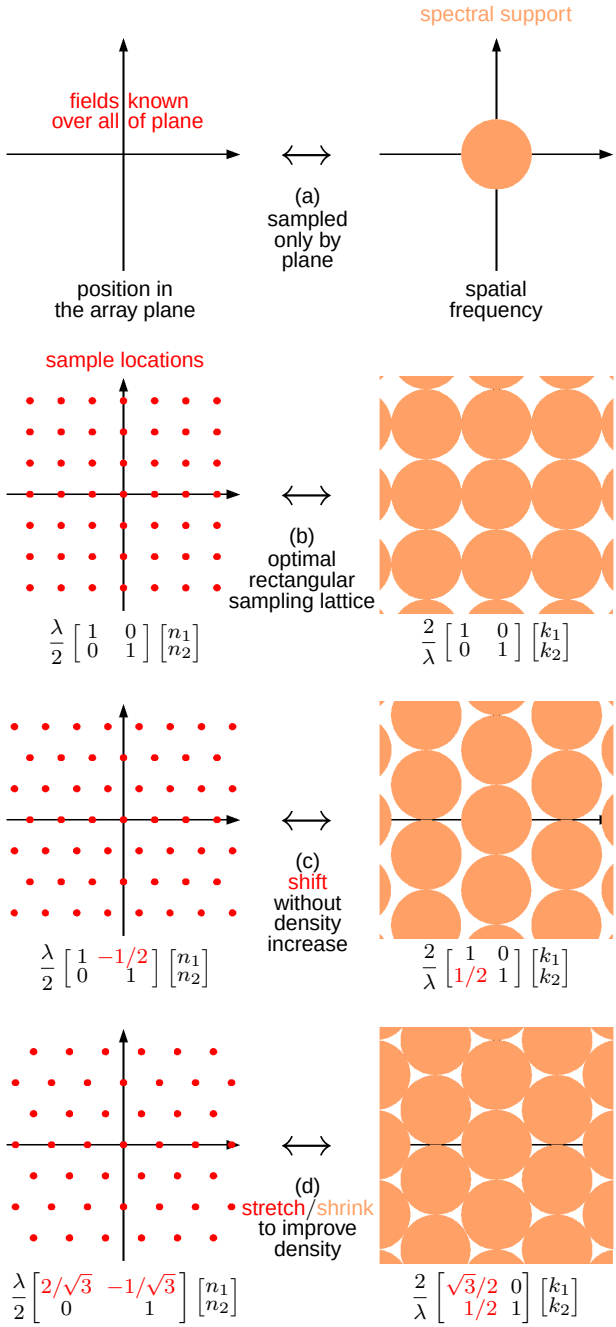

Figure 3: Here 2D Fourier pairs represent spatial sampling, with position in the array plane and 2D spatial frequency represented on the left and right respectively. Unsampled (except by the plane) case (a) evolves to the optimal rectangular array (b) and, in separate shifting (c) and scaling (d) steps, to the optimal triangular array.

system used for the transform, there may be scaling as well as replication, but that is unimportant here. The sampling-interval and spectral-period matrices are inverse transposes of each other. If samples on a square grid are spaced further apart than the $\lambda/2$ case shown, the spectral replicas overlap, resulting in the well-understood grating-lobe phenomenon.

Array cost increases with sample density in the plane,

because samples represent element locations, and therefore decreases as spectral replicas are packed more densely in spatial frequency. To prepare to increase this packing efficiency, in Fig. 3(c) we adjust the spectral-period matrix to slide columns of spectral replicas vertically. This changes the sample-interval matrix so as to slide sample rows horizontally. Sample-point and replica-offset densities are unchanged, but spectral space on the right is more available. In Fig. 3(d) we then modify the spectral-period matrix to shrink the horizontal components of translate spacings until the replicas just touch. This changes the sample-interval matrix so as to stretch sample spacing horizontally until sample positions are related by equilateral triangles. This triangular lattice (often called the hexagonal lattice) is $\sqrt{3}/2$ as dense as (about 13.4% less dense than) the square lattice of Fig. 3(a) and is widely used in planar arrays.

3: Sampling in 3D Spacetime

The approach used above in 2D to derive the triangular sampling lattice will now be used in 3D to arrive at the new array-sampling scheme. Spatial frequency was represented in Fig. 2 in the horizontal plane and was assumed associated with signals having $|f|$ fixed. We can extend this incident-signal representation to 3D by using the vertical axis for frequency f. The narrowband case results in the spectral support pictured in Fig. 4(a), shown at "$\pm f$" because real signals comprise complex exponentials in conjugate pairs with frequencies mirrored through the spectral origin, even in this 3D representation. In the Fig. 4(b) wideband case in which signals with frequencies up to $|f|$ in magnitude are passed by the element pattern and receiver front end, the 3D support region extends from one circle to the other. Because its spatial radius is proportional to the absolute value of temporal frequency (see Fig. 2), the 3D spectral-support region takes the shape of a double cone.

The Fig. 4(b) spectral-support diagram would be different for bandpass sampling or if frequency translation were involved, and it would have to be augmented if aliasing were allowed into guard bands in f or if grating lobes were allowed in spatial frequency. The former is natural when filter transition bands are considered, and the latter is acceptable if the pattern's main beam will never be scanned to the $90°$ limit from boresight. Both options increase spectral packing density and thereby decrease cost. Such considerations are addressed elsewhere [2] for the linear array, and the methods described there would largely transfer to the planar array. However, because of the multidimensional complexity involved, no simply elaborated "Nyquist rule" is really adequate for the planar array, and the specific tradeoff to be derived next should not be taken as one. The spectrum-packing analysis, such as is about to follow, must be carefully repeated for each specific design.

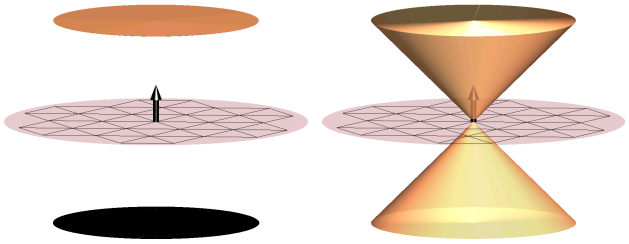

(a) narrowband case (b) wideband case

Figure 4: Spectral support of incident plane waves in 3D frequency.

3.1: Spectral-Replica Packing in 3D

The 2D argument of Fig. 3 is extended to 3D in Fig. 5. Each diagram (a)–(g) depicts a Fourier pair as before, but now in 3D with the new axes being, on the left, a time axis extending out of the page towards the reader and, on the right, a vertical f axis as in Fig. 4. Unsampled case (a) supposes signals are known over the entire array plane over all time. Diagram (b) then depicts sampling in space only, on the triangular sampling lattice derived in Fig. 3. Each gray circle on the left schematically denotes a line extending infinitely into and out of the page to represent knowledge of the input at one point in the plane but at all times. This spatial sampling infinitely replicates the spectral support horizontally, leaving the cones just touching to make Fig. 5(b) a 3D version of Fig. 3(d). The new 3D frequency domain in Fig. 5(b) is viewed from a point that in Fig. 3(d) would be to the lower right and just above the page.

Now let us sample in time as well. Sampling at rate $T^{-1} = 2|f| = \frac{c}{\lambda/2}$ in Fig. 5(c) causes the spectra to replicate vertically and just touch. Only a few cones are shown, but replication continues infinitely in all directions. Sampling in time is not visible here graphically, but we can imagine it well enough. The sample-interval and spectral-period matrices are now each 3×3 and block diagonal to reflect that time and space are sampled separately, in conventional fashion. The sample-interval and spectral-period matrices are in fact those of Fig. 3(d), augmented now with a new row and a new column each, and samples in time and replica offsets in f are indexed by new variables n_3 and k_3 respectively. Just as with spatial sampling on the square lattice in Fig. 3(b), the spectral-support regions here touch at their widest points and leave much of the spectrum empty.

Everything in the paper to this point can be considered background, discussion to establish context and notation. Only now does something really new happen.

On the right in Fig. 5(d) columns of cones have been displaced vertically by modifying the spectral-period matrix. The column of cones indexed by pair (k_1, k_2) is displaced in frequency by $0.17(k_1 - k_2)$, with the proportionality constant set simply to illustrate that at each successive

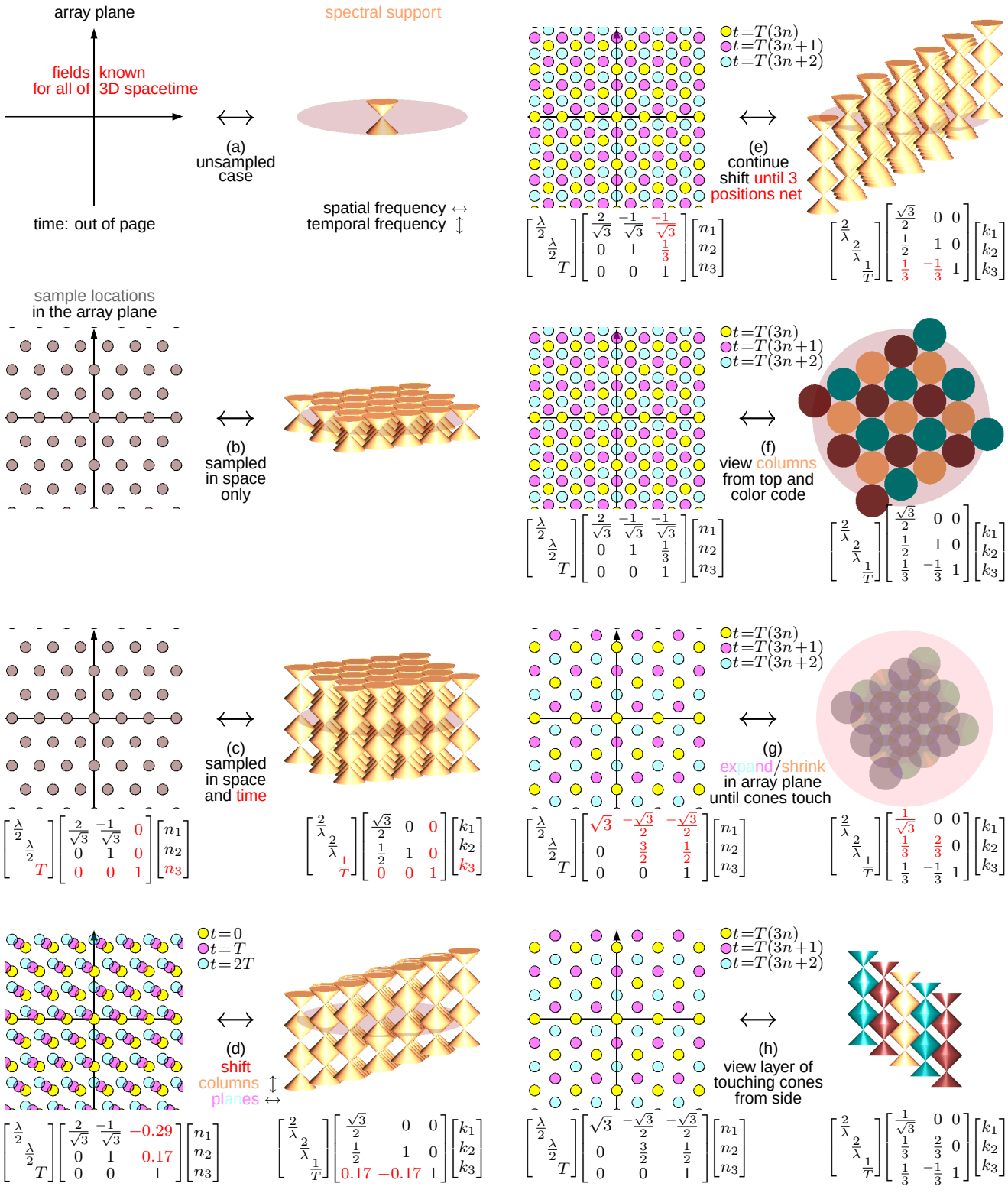

Figure 5: This development parallels that of Fig. 3 but in 3D. Two spatial dimensions (the array plane) and one temporal dimension t on the left are matched on the right by two spatial-frequency dimensions and one temporal-frequency dimension f.

sampling instant, *i.e.* as time index n_3 on the left is stepped, sample positions in space are displaced further and further along an axis 30° from the horizontal. In Fig. 5(d) the wide parts of the cones on the right display a potentially useful vertical misalignment, but the sampling scheme on the left is as yet impractical because it would require a hugely increased set of array elements. In Fig. 5(e), however increasing the relevant proportionality constant has made the set of spatial positions used periodic with period three. Element density is now $3\times$ higher than originally, but the A/D clocking rate at each element is now $1/3$ as fast.

If the columns on the right Fig. 5(e) were cylinders rather than cones (as would likely be the case when sampling more widely spaced subarray outputs) this 3:1 tradeoff would be the end of the matter. But the per-element RF sampling here has given us cones, and so on the right the columns no longer touch. Empty space waits to be claimed. In Fig. 5(f) nothing is changed from Fig. 5(e) except the viewpoint from which we look at the cones on the right, now viewed from above (with page vertical here corresponding to page left in Fig. 3(d)). The columns of cones here have now been color coded according to net displacement vertically relative to the center column, still copper colored, which of course remains unshifted. Other columns still copper colored have been shifted by an integral multiple of a cone height, one vertical period, and so in the net are not shifted at all. Likewise, once integral periods are ignored all the maroon columns have the same net shift, as do all the blue columns. One of those noncopper colors represents a net $1/3$ cone-height shift upward, the other a net $1/3$ cone-height shift downward ($2/3$ upward).

Viewed from above, the cone columns in Fig. 5(f) appear to touch, but this is an illusion. No column has the same net vertical displacement as any of its neighbors, so there is empty space between them. In Fig. 5(g) the first two rows of the spectral-period matrix have each been scaled by $\frac{2}{3}$, reducing all replica offsets by a third on the right, which amount reduces their spacing just to the point where the columns of cones first touch. The wide parts of the cones are no longer aligned vertically, so viewed from the top there appears to be overlap, but side view (h) shows this to be illusory. On the left in (g) the first two rows of the sample-interval matrix have each been scaled by $\frac{3}{2}$, lowering the element density in the plane (and the cost, more or less) by $\left(\frac{3}{2}\right)^2 = \frac{9}{4}$ to reveal the final configuration proposed.

4: Summary and Conclusions

Table 1 summarizes the performance obtained. Compared to the optimal conventional configuration in which elements spaced at $\lambda/\sqrt{3}$ (at the top of the RF band) on a triangular lattice are sampled simultaneously, the proposed three-phase array-sampling approach requires $4/3$ the element density but only $1/3$ the A/D clocking rate (given a fixed upper band edge). This tradeoff would appear to be very useful in wideband systems for radar and electronic surveillance for which available A/D technology is the limiting factor in available design bandwidth.

f_s = individual A/D rate

λ = wavelength at upper band edge

scheme	*band edge*	*element spacing*	*element density*
• square grid ordinary sampling	$\frac{f_s}{2}$	$\frac{\lambda}{2}$	$\frac{4}{\lambda^2}$
• triangular grid ordinary sampling	$\frac{f_s}{2}$	$\frac{\lambda}{\sqrt{3}}$	$\frac{2\sqrt{3}}{\lambda^2}$
• triangular grid three-phase sampling	$3\times\frac{f_s}{2}$	$\frac{\lambda}{2}$	$\frac{4}{3}\times\frac{2\sqrt{3}}{\lambda^2}$

Table 1: Performance comparison.

Not addressed specifically in this paper but immediately accessible through a parallel development is perhaps the most important practical case, that of a 2D array on a square grid, where if element locations are colored as on a chess board, red and black element groups can be sampled alternately in a two-phase sampling scheme. Relative to ordinary, simultaneous sampling of optimally placed array elements on square grid, such a scheme halves the A/D clocking rate without increasing element density at all.

Higher clock-rate reduction factors are also possible. In Fig. 5(e) matrix coefficients are set so that $N = 3$ time steps move the sample from the spatial origin to a "target point" offset from it by $\sqrt{N}$ times the original element spacing. A future paper will argue that any target point $\sqrt{N}$ times further from the origin than the origin's nearest neighbor can be used if N is prime. This means that N-phase sample timing can be used on the triangular grid for $N \in \{3, 7, 13, 19, \ldots\}$ and on the square grid for $N \in \{2, 5, 13, 17, \ldots\}$. The tradeoff between element density and A/D clock rate is less favorable as N increases.

References

[1] T. Ajdler and M. Vetterli, "The plenacoustic function, sampling and reconstruction," in *IEEE Conf. on Acoustics, Speech and Signal Processing* (Hong Kong), Apr. 2003.

[2] J. O. Coleman, "Ping-pong sample times on a linear array halve the Nyquist rate," in *IEEE International Conference on Speech, Acoustics, and Signal Processing*, Montréal, Canada (http://www.icassp2004.com/), May 2004.

[3] J. O. Coleman and D. P. Scholnik, "Beam Design for a Ping-Pong-Sampled Linear Receive Array," in *12th European Signal Processing Conference*, Vienna, Austria (http://www.nt.tuwien.ac.at/eusipco2004/), Sept. 2004.